PCCP

ROYAL SOCIETY OF CHEMISTRY

PAPER

View Article Online
View Journal | View Issue

Cite this: *Phys. Chem. Chem. Phys.*, 2025, **27**, 4728

Energy decomposition analysis for excited states: an extension based on TDDFT†

Florian Kreuter and Ralf Tonner-Zech *

To enhance the understanding of photochemical reactivity and its mechanisms, it is essential to analyze bonding interactions in excited-state reactions. Such insights can aid in optimizing these reactions. This paper presents an energy decomposition analysis method for excited states (exc-EDA), integrating the ground state EDA approach by Morokuma, Ziegler and Rauk with time-dependent density functional theory (TDDFT). The methodology focuses on calculating excitation energies, particularly for the intermediate states of the EDA. We introduce two variants: the first uses non-relaxed excitation coefficients (exc-u-EDA), where the excitation coefficients of the excited fragment are used directly; the second optimizes these coefficients for the intermediate states (exc-r-EDA). Exc-EDA can be applied with various density functionals, but the accuracy depends on the functional's ability to describe the excited state properly. Smaller basis sets result in lower energy values due to fewer virtual orbitals, while larger basis sets produce consistent relative results but may involve different excited states in intermediate steps leading to artificial increase of energy terms in the EDA. The method's convergence behavior resembles that of TDDFT, with a computational cost approximately three times that of the underlying TDDFT calculation. At the current stage, the method requires that the excitation is localized on one of the fragments, but it also enables an analysis of the subsequent charge-transfer effects. Application of exc-EDA to singlet fission in pentacene clusters demonstrates its practical value, offering quantitative insights into excited-state bonding and revealing clear, intuitive trends.

Received 4th November 2024,
Accepted 8th February 2025

DOI: 10.1039/d4cp04207g

rsc.li/pccp

1. Introduction

The excited state of molecules is highly relevant in various research fields like photochemistry, solar to chemical energy conversion, and photocatalysis.[1] Here, molecules not only exhibit an electronic but also an atomic structure distinct from the ground state, enabling reactions that are not possible in the ground state.[2] Often, chemical interactions in the excited state are decisive for conversion efficiency or selectivity.[3] It would be highly beneficial to quantify these interactions with an electronic structure analysis method and be able to derive trends and predict new avenues for experiment. Such a bonding analysis method would allow for a more comprehensive understanding of the reactivity, including the mechanisms underlying photochemical reactions. There are several theoretical approaches[4] for the description of excited states, including multi-reference methods[5] such as complete active space SCF (CASSCF),[6] complete active space perturbation theory of second order (CASPT2),[7] *n*-electron valence state perturbation theory (NEVPT2),[8] multireference CI (MRCI)[9] and restricted active space SCF (RASSCF).[10] Single-reference calculations[2,4] can be performed using coupled cluster (CC) approaches[11] like equation-of-motion CC (EOM-CC)[12] or approximate second-order CC (CC2),[13] but also the algebraic diagrammatic construction (ADC),[14] full configuration interaction (FCI) and time-dependent density functional theory (TDDFT).[2,15,16] TDDFT is the most efficient method for calculating excitation energies and experimental spectra.[2] It also has the advantage of being a 'black-box' method, making it more user-friendly compared to other methods, particularly the multi-reference methods.[4] Therefore, TDDFT is the most used method for calculating excited states in molecular chemistry. Conversely, TDDFT encounters difficulties with long-range charge transfer (CT) excitations, double excitations, and Rydberg excitations.[2,4,16] The challenges of TDDFT with CT and Rydberg excitations are primarily attributed to the semilocality of the underlying density functionals. In the derivation of linear response (LR-)TDDFT, only single excitations are considered, which explains the issues with double excitations.

The character of chemical bonds is often analyzed to understand chemical reactions and trends. One major approach is energy decomposition analysis (EDA).[17] In this method, the system is divided into two fragments, with the bond being analyzed between them (Fig. 1). EDA then divides the bonding energy into distinct contributions, which can be chemically

Wilhelm-Ostwald-Institut für Physikalische und Theoretisch Chemie, Universität Leipzig, Linnéstr. 2, 04103 Leipzig, Germany. E-mail: ralf.tonner@uni-leipzig.de

† Electronic supplementary information (ESI) available. See DOI: https://doi.org/10.1039/d4cp04207g

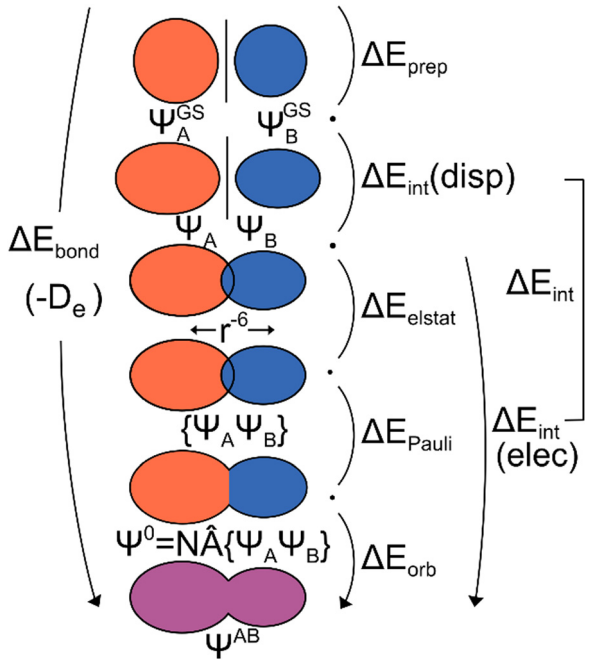

Fig. 1 Schematic representation of the ground state EDA (adapted from ref. 22).

interpreted. For the EDA based on developments by Morokuma and the related extended transition state method by Ziegler and Rauk (jointly called EDA in the following) these are electrostatic interactions between charge densities of fragments, Pauli repulsion, and orbital interaction.[18–21] We will use this method as a starting point for our development.

Further EDA and EDA-type methods comprise generalized Kohn–Sham-EDA (GKS-EDA),[23] interacting quantum atoms (IQA),[24] block-localized wave function (BLW) EDA[25] and its variant the absolutely localized molecular orbital EDA (ALMO-EDA),[26] generalized product function (GPF) EDA,[27] natural EDA (NEDA)[28] and localized molecular orbital (LMO) EDA.[29] These methods are either based on the determination of the electron density or orbital space. Additionally, there are EDA methods based on perturbation theory, such as symmetry-adapted perturbation theory (SAPT).[30] The use of EDA methods allows for the investigation of a multitude of inter- and intramolecular bond types, including those of a covalent nature observed in organic molecules[20] and ligand–metal interactions observed in transition metal complexes.[20] Additionally, hydrogen bonds, donor–acceptor bonding, and other interactions can be analyzed. To obtain a more precise picture of the orbitals involved in the respective bond, the natural orbital for chemical valence (NOCV) extension[21] for the EDA was developed by Mitoraj and Ziegler. The orbital contribution in deformation densities formed by the NOCVs, which visualizes the charge flow during bond formation, can thus be decomposed further. In addition to molecular systems, energy decomposition analysis for extended systems (pEDA)[22] can be used to understand bonding questions in surface and material science.[31] The activation strain model (ASM)[32] employs the EDA for the precise investigation of reactivity. This model splits the energies along the reaction path into the reaction stress (deformation of the reactants) and an interaction contribution.[33]

However, most of these methods are applicable to the electronic ground state only. So far, only ALMO-EDA,[34] GKS-EDA,[35] and density functional-based tight binding EDA (DFTB-EDA),[36] have been extended to treat excited states. ALMO-EDA splits the bonding energy into frozen, polarization, and charge transfer terms. The frozen contribution can be approximately matched to the sum of Pauli repulsion and electrostatic interaction in EDA. The ALMO-EDA for the excited state obtains the contributions by calculating the changes caused by the electronic excitation and adding them to the contributions in the ground state. For the calculation of the excitation, configuration interaction single (CIS)[2] or the similar TDDFT method with Tamm–Dancoff approximation (TDA) can be used. DFTB-EDA is a semiempirical method that is efficient but less accurate. GKS-EDA splits the bonding energy into electrostatic, exchange-repulsion, polarization, and correlation contributions. The extension to excited states is based on the fact that each intermediate wave function is constructed as a linear combination of simply excited determinants. A further method is the multistate energy decomposition analysis (MS-EDA) method.[37] It breaks down the formation reaction of an excimer into different thermodynamic intermediate steps.

What is common to all methods for excited state bonding analysis is that they can be used for exciplex or excimer systems only, where the bonding results from the electronic excitation of one fragment.[38] The reason is that choosing the excited fragment is (mostly) straightforward in these systems while the second fragment stays in the ground state. Our development will follow the same approach. A different angle is taken by Kimber and Plasser:[39] their approach splits the excitation energy into orbital energy differences, coulomb attraction between hole and electron, repulsive exchange interaction, and exchange correlation (XC)-contributions.

In addition to the EDA methods, natural transition orbitals (NTO)[40] are used to understand excited states. Similar to the natural bond orbital (NBO) approach[41] for the ground state, NTO is a reduction of the orbital space. This reduces the excitation to mostly one or a few transitions between localized orbitals, as opposed to the mixed character resulting from the canonical orbital picture. Furthermore, the orbitals involved in the excitation can be visualized using the adaptive natural density partitioning method.[42] Additionally, various qualitative descriptors for charge CT[43] and double excitation[44] are in use.

For the ground state, many studies have successfully applied the EDA method to better understand chemical bonding. These studies range from chemical bonding in small main group compounds[18,20] to the analysis of donor–acceptor bonds in Lewis acid–base adducts[45] and the study of ligand–metal interactions in transition complexes.[46] This method has also been used, for example, to study the influence of aromaticity[47] on the bonds in benzene. More exotic bonds were also analyzed like halogen,[48,49] chalcogen,[48,50] and pnictogen[48,51] bonding, the interactions between alkali metal cations with hydrides[52] and host–guest interactions in heterocalixarenes.[53]

What is lacking is an extension of this powerful analysis method to the excited state. Here, we show how the EDA scheme can be combined with TDDFT to achieve this goal. This excited state EDA (exc-EDA) is based on the calculation of the excitation energy for the intermediate states. Aside from the theoretical foundation, test systems are presented to identify the computational approach for using the method efficiently. As an application-oriented example, pentacene clusters, a relevant system for singlet fission, is analyzed with the exc-EDA method.

2. Theory

2.1. Ground state EDA

The use of EDA allows for the determination of the character of a chemical bond by breaking down the bonding energy ΔE_{bond} into chemically interpretable contributions. This is achieved by dividing the system AB into two fragments, A and B. We use the generic term 'system' for AB which can be two molecular fragments, a molecule and a surface, *etc.* The bonding energy ΔE_{bond} is equivalent to the negative dissociation energy D_e and represents the energy difference between the system E_{AB} and the relaxed fragments A (E_{A}^{GS}) and B (E_{B}^{GS}) (eqn (1)).

$$\Delta E_{\text{bond}} = E_{\text{AB}} - E_{\text{A}}^{\text{GS}} - E_{\text{B}}^{\text{GS}} = -D_e \tag{1}$$

To break down the bond energy into its various components, the EDA introduces intermediate stages of bond formation (Fig. 1). The initial step involves deforming the fragments from their optimized structure ($\Psi_{\text{A}}^{\text{GS}} + \Psi_{\text{B}}^{\text{GS}}$) to the structure in the system ($\Psi_{\text{A}} + \Psi_{\text{b}}$). This process also considers the change in electronic state if applicable. The preparation energy ΔE_{prep} summarizes all these effects, representing the energy difference between the fragments in the system structure and the ground state structure (eqn (2)).

$$\Delta E_{\text{prep}} = E_{\text{A}} + E_{\text{B}} - E_{\text{A}}^{\text{GS}} - E_{\text{B}}^{\text{GS}} \tag{2}$$

The 'prepared' fragments are then bonded with the attractive interaction energy ΔE_{int}. It is the central quantity in the EDA and summarizes all interactions between the fragments. In a first step, it can be split into an electronic ΔE_{int}(elec) and a dispersion term ΔE_{int}(disp) (eqn (3)).

$$\Delta E_{\text{bond}} = \Delta E_{\text{prep}} + \Delta E_{\text{int}} = \Delta E_{\text{prep}} + \Delta E_{\text{int}}(\text{disp}) + \Delta E_{\text{int}}(\text{elec}) \tag{3}$$

The dispersion contribution ΔE_{int}(disp) simply reflects the difference in dispersion interaction between the system and the ground state fragments. The calculation of the respective interactions uses dispersion correction methods (mostly DFT-D3[54]). As the dispersion energy of such semiempirical methods depends only on the atomic arrangement, it is not considered in the next section for the extension of EDA to excited states since we are only interested in vertical excitations where atomic structure does not change.

To further decompose the electronic part of the interaction energy ΔE_{int}(elec), we start by setting the separately calculated charge densities of the fragments to the equilibrium distance. That leads to the Coulomb interaction between the charge densities: the quasiclassical electrostatic contribution ΔE_{elstat} (eqn (4)). For most bonds, the attractive interaction of the electron density of one fragment with the positive nuclei of the other fragment (2nd and 3rd term in eqn (4)) outweighs the nuclei–nuclei (1st term) and electron–electron repulsion (4th term), making this contribution attractive.

$$\begin{aligned}\Delta E_{\text{elstat}} = &\sum_{\alpha\in\text{A}}\sum_{\beta\in\text{B}}\frac{Z_\alpha Z_\beta}{|R_\alpha - R_\beta|} + \sum_{\alpha\in\text{A}}\int\frac{Z_\alpha\rho_{\text{B}}(r_i)}{|R_\alpha - r_i|}\mathrm{d}r_i \\ &+ \sum_{\beta\in\text{B}}\int\frac{Z_\beta\rho_{\text{A}}(r_i)}{|R_\beta - r_i|}\mathrm{d}r_i + \iint\frac{\rho_{\text{A}}(r_i)\rho_{\text{B}}(r_j)}{|r_i - r_j|}\mathrm{d}r_i\mathrm{d}r_j\end{aligned} \tag{4}$$

This step results in the product wave function $\{\Psi_{\text{A}}\Psi_{\text{B}}\}$. However, this wave function violates the Pauli principle and must be antisymmetrized and normalized to the intermediate wave function $\Psi_0 = N\hat{A}\Psi_{\text{A}}\Psi_{\text{B}}$ in the next step. This leads to a constraint on the wave function and a repulsive contribution known as Pauli repulsion ΔE_{Pauli} (eqn (5)).

$$\Delta E_{\text{Pauli}} = E(\Psi_0) - E(\{\Psi_{\text{A}}\Psi_{\text{B}}\}) \tag{5}$$

The final step involves relaxing the orbitals from the antisymmetrized intermediate state Ψ_0 to the orbitals in the system (eqn (6)). This term is called orbital contribution ΔE_{orb}. It is always attractive for ground state EDA and contains charge transfer and polarization contributions.

$$\Delta E_{\text{orb}} = E_{\text{AB}} - E(\Psi_0) \tag{6}$$

The electronic interaction energy ΔE_{int}(elec) is then the sum of the quasi-electrostatic ΔE_{elstat}, Pauli repulsion ΔE_{Pauli}, and orbital contribution ΔE_{orb} (eqn (7)).

$$\Delta E_{\text{int}}(\text{elec}) = \Delta E_{\text{elstat}} + \Delta E_{\text{Pauli}} + \Delta E_{\text{orb}} \tag{7}$$

2.2. Extension to use one excited state fragment

The exc-EDA similarly divides the system into two fragments to investigate their bonding interactions quantitatively. Currently, exciplexes can be analyzed where one fragment is excited (A*) while the other remains in the ground state (B). The excitation of fragment A* results in a bond between the two fragments. This approach has the advantage of unambiguous fragment assignment and has been used in all other excited state EDA approaches up to now. The exc-EDA uses the interaction energy ΔE_{int}^* as the central term, which is decomposed. ΔE_{int}^* can be determined by calculating the energy difference between the excited system (AB)* and the sum of excited fragment A* and ground state fragment B (eqn (8)).

$$\Delta E_{\text{int}}^* = E_{\text{AB}}^* - E_{\text{A}}^* - E_{\text{B}} \tag{8}$$

The asterisk (*) indicates that the excited state is considered for these energies. It should be noted that only vertical excitations are used when calculating the interaction energy, as structural effects are not considered. This means that the fragments have the same structure as the ground state structure

of the system. With this choice we focus on the electronic changes upon excitation without obscuring geometrical relaxations that follow. Additionally, the interaction energy ΔE^*_{int} for the excited states can be separated into a ground state component $\Delta E^{\text{GS}}_{\text{int}}$ and an excitation component ω_{int}.

$$\Delta E^*_{\text{int}} = \Delta E^{\text{GS}}_{\text{int}} + \omega_{\text{int}}, \omega_{\text{int}} = \omega_{\text{AB}} - \omega_{\text{A}} \tag{9}$$

For the remainder of the paper, the energy terms for the excited states are denoted by E^*_i, while the ground state contributions are denoted by E^{GS}_i. The changes in energy terms due to excitation are denoted by ω_i. Additionally, eqn (9) shows that ΔE^*_{int} describes the change in excitation of fragment A* resulting from interactions with fragment B.

As described in the previous section, we only use dispersion interaction for the ground state (eqn (10)), as the method used (DFT-D3) is only dependent on structure and we consider vertical excitations, only. Conversely, the density and polarizability change during excitation, which then naturally causes changes in dispersion interactions. However, it should be noted that none of the dispersion correction methods that take the electron density explicitly into account is available for excited states up to now. In the future, our method could be extended if a suitable density-dependent dispersion correction approach is available.

$$\begin{aligned} \Delta E^*_{\text{int}} &= \Delta E^*_{\text{int}}(\text{elec}) + \Delta E^{\text{GS}}_{\text{int}}(\text{disp}) \\ \omega_{\text{int}} &= \omega_{\text{int}}(\text{elec}) \end{aligned} \tag{10}$$

A scheme visualizing exc-EDA is shown in Fig. 2.

As can be seen in Fig. 2, the new method is based on calculating the excitation energy for the two intermediate states (product state $\omega(\Psi^*_{\text{A}}\Psi_{\text{B}})$ and antisymmetrized state $\omega(\Psi^*_0)$). Moreover, Fig. 2 illustrates the product and antisymmetrized wave function for the excited states in a manner analogous to that employed for the ground state. Then, the excitation energy ω (orange in Fig. 2) is calculated based on these ground state wave functions, where we use the respective ground state orbitals. Analogous to calculating the contributions for the ground state, the excited state contribution ΔE^* and excitation contribution ω are calculated by the difference of excited state energy resp. excitation energy of the corresponding states. Eqn (11) shows the LR-TDDFT approach in matrix representation.[2]

$$\begin{bmatrix} \mathbf{A} & \mathbf{B} \\ \mathbf{B}^* & \mathbf{A}^* \end{bmatrix} \begin{bmatrix} \mathbf{X} \\ \mathbf{Y} \end{bmatrix} = \omega \begin{bmatrix} 1 & 0 \\ 0 & -1 \end{bmatrix} \begin{bmatrix} \mathbf{X} \\ \mathbf{Y} \end{bmatrix}, \text{ with}$$
$$A_{ia,jb} = \delta_{ij}\delta_{ab}(\varepsilon_a - \varepsilon_i) + (ia|jb) + (ia|f_{\text{xc}}|jb) \tag{11}$$
$$B_{ia,jb} = (ia|bj) + (ia|f_{\text{xc}}|bj)$$

Here, matrix **A** describes the excitation effects, matrix **B** the de-excitation effects, and higher-order correlation effects. **X** is the excitation vector corresponding to **A**, and **Y** is the de-excitation vector corresponding to **B**. The ω values are the eigenvalues of the TDDFT eigenvalue problem (eqn (11)), which correspond to the excitation energy. To calculate matrices **A** and **B**, it is necessary to know the orbital energies ε_i and ε_a, the two-electron integrals $(ia|\,jb)$ and the exchange–correlation contribution $(ia|\,f_{\text{xc}}|\,jb)$. If all orbitals are real, this allows us to transform eqn (11) into a normal eigenvalue problem (eqn (12)).[2]

$$\begin{aligned} \Omega\mathbf{Z} &= \omega^2\mathbf{Z}, \text{ with} \\ \mathbf{\Omega} &= (\mathbf{A}-\mathbf{B})^{1/2}(\mathbf{A}+\mathbf{B})(\mathbf{A}-\mathbf{B})^{1/2} \\ \mathbf{Z} &= (\mathbf{A}-\mathbf{B})^{-1/2}(\mathbf{X}+\mathbf{Y}) \end{aligned} \tag{12}$$

In this context, $\mathbf{\Omega}$ represents the summarized excitation matrix, while **Z** represents the corresponding excitation vector. Another way to convert eqn (11) into a normal eigenvalue problem is to use TDA.[55] This approximation neglects the **B**-matrix, which describes de-excitation. As the values of **B** and **Y** are usually very small,[55] this is a good approximation. The

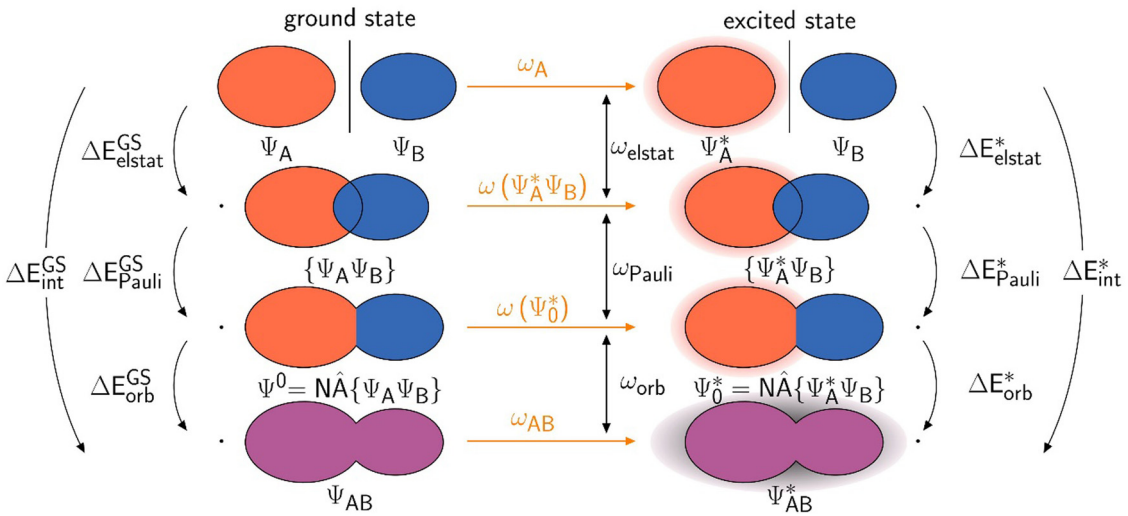

Fig. 2 The decomposition of the interaction energy of exc-EDA between fragments A and B for the ground state (left) and the excited state (right). The excitations of fragment A and the system are indicated by the shading, whereby the respective excitation energies are orange.

eigenvalue problem to be solved in the TDA is shown in eqn (13).

$$\mathbf{AX} = \omega\mathbf{X} \tag{13}$$

Exc-EDA can be used with or without TDA. Eqn (11)–(13) show that the orbital energies ε_i and orbitals ϕ_i are required to calculate the excitation energy ω. The orbitals ϕ_i are used to determine both the exchange–correlation contribution and the two-electron integrals. To this end, we use the respective orbitals ϕ_i from ground state EDA intermediate steps. Since the orbital energies ε_i of the intermediate steps are not calculated in the currently available implementation of ground state EDA, we determine them within the newly developed method. To do this, we construct the Fock matrix from the respective orbitals for the intermediate states and then transfer it to the MO basis. The Fock matrix is approximately diagonalized using the overlap matrix. If the Fock matrix is completely diagonalized, the new coefficients result in states that go beyond those considered in the EDA. Furthermore, the exc-EDA method does not require an exact calculation of the excitation energy as it works on the basis of a model state. For its purposes, an approximate excitation energy is sufficient, which can be calculated efficiently with this method. We then use the diagonal elements as an approximation for the orbital energies ε_i.

There are two different approaches for calculating the excitation energy ω for the intermediate states. The first is in the spirit of the original EDA that all orbital interactions are summarized in the orbital contribution ΔE_{orb}. Thus, the excitation vector $\mathbf{Z}$ resp. $\mathbf{X}$ must not contain any contributions for excitation between the fragments. To achieve this, we construct the excitation vector $\mathbf{Z}$ ($\mathbf{X}$) from the excitation vectors $\mathbf{Z}_{\mathrm{A}}$ ($\mathbf{X}_{\mathrm{A}}$) of the fragments. This approach does not change the excitation coefficients for the two intermediate states. This is why the method is referred to as ''unrelaxed coefficients'' (exc-u-EDA). We then determine the respective excitation energy ω_i for the intermediate states by calculating the matrix-vector product between the excitation vector $\mathbf{Z}$ ($\mathbf{X}$) and the excitation matrix $\boldsymbol{\Omega}$ ($\mathbf{A}$) (eqn (14)).

$$\begin{aligned}\text{without TDA:}\omega_i &= \mathbf{Z}^{\mathrm{T}}\boldsymbol{\Omega}_i\mathbf{Z}\\ \text{with TDA:}\omega_i &= \mathbf{X}^{\mathrm{T}}\mathbf{A}_i\mathbf{X}\end{aligned} \tag{14}$$

The intermediate states determined with this variant are more similar to the fragments, which means that all excitations between the fragments are summarized in the orbital contribution. This makes the orbital contribution quite large, especially when there is charge transfer between the fragments.

The other variant we implemented is based on a standard way of calculating excitation energies. Here, the intermediate states are constructed for the ground state, and then the excitation energy ω_i is calculated based on these intermediate states. In this variant, the orbitals ϕ_i and orbital energies ε_i for the respective intermediate state are used to build up the excitation matrix $\boldsymbol{\Omega}$ resp. $\mathbf{A}$. The eigenvalues of this matrix, or excitation energy ω_i, are then determined using the Davidson approach.[56] This changes the excitation coefficients, which is why this variant is referred to as ''relaxed coefficients'' (exc-r-EDA). This means that excitations between the fragments are already accounted for in the product wave function, which makes the intermediate states more similar to the relaxed full system (AB)*. Charge transfer effects are thus distributed over the different EDA terms. For this reason, this variant is more suitable for systems with considerable charge transfer. Fig. 3 shows the implementation of the method schematically.

Initially, exc-EDA performs the calculations for the fragments, utilizing TDDFT for fragment A and (ground state) DFT for fragment B (Fig. 3). Subsequently, a TDDFT calculation is done for the system (AB)*. Thereafter, the excitations for the two intermediate steps are calculated with both variants (Fig. 3). Finally, the actual EDA excitation contributions ω_i are calculated from the differences between the excitation energies of the intermediate states (Fig. 3). The EDA term for the excited state ΔE_i^* is obtained by adding the ground state values ΔE_i^{GS} (eqn (15)).

$$\Delta E_i^* = \omega_i + \Delta E_i^{\mathrm{GS}} \tag{15}$$

Therefore, the quasi-electrostatic excitation contribution ω_{elstat} is equal to the difference between the excitation energy of the product wave function ($\omega(\{\Psi_{\mathrm{A}}\Psi_{\mathrm{B}}\})$) and the excited fragment A (ω_{A}) (eqn (16)).

$$\omega_{\mathrm{elstat}} = \omega(\{\Psi_{\mathrm{A}}\Psi_{\mathrm{B}}\}) - \omega_{\mathrm{A}} \tag{16}$$

This contribution ω_{elstat} describes the changes in Coulomb interaction due to the excitation of fragment A. In particular, the relaxed variant can lead to larger contributions due to charge transfer between the fragments. This can result in partial charge differences, which leads to an increase of electrostatic interaction. If an initial charge difference is equilibrated by charge transfer, it can also lead to a decrease in electrostatic interaction due to the excitation.

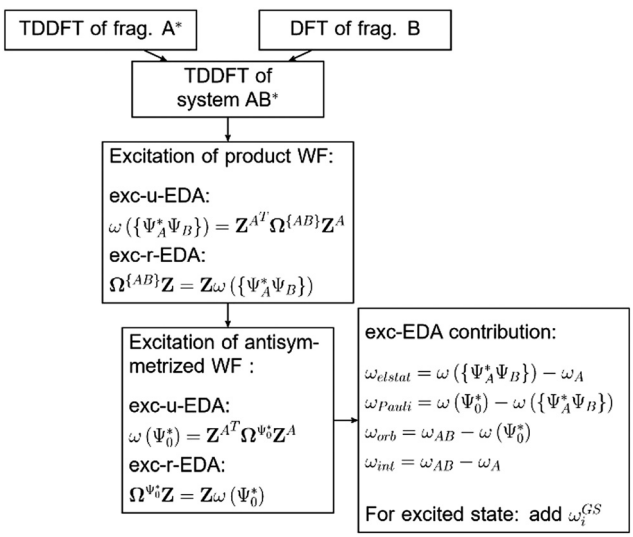

Fig. 3 Flow scheme for implementation of exc-EDA.

Next, the Pauli excitation contribution ω_{Pauli} corresponds to the change in excitation energy between the antisymmetrized $\omega(\Psi_0)$ and product wave functions $\omega(\{\Psi_A\Psi_B\})$ (eqn (17)).

$$\omega_{\text{Pauli}} = \omega(\Psi_0) - \omega(\{\Psi_A\Psi_B\}) \quad (17)$$

The magnitude of this contribution is primarily determined by the shift in electron density during excitation. An increase in electron density in the bonding region leads to an enhancement of Pauli repulsion, while a decrease in electron density in the overlapping region of the fragments results in a weaker Pauli repulsion.

Finally, the orbital excitation contribution ω_{orb} is the excitation energy difference between the system and the antisymmetrized wave function $\omega(\Psi_0)$ (eqn (18)).

$$\omega_{\text{orb}} = \omega_{AB} - \omega(\Psi_0) \quad (18)$$

As previously stated, the orbital contribution for the unrelaxed variant can become quite large. Note that the usual trends for ground state EDA interaction terms (electrostatic and orbital interaction are attractive, Pauli repulsion is repulsive) are not necessarily true for the change upon excitation as outlined above.

3. Computational details

All calculations were performed using a developer's version of the ADF module in the Amsterdam modeling suite (AMS) program package.[57] To test the exc-EDA method, the bonding in the complexes fluorenone*–methanol, quinoline*–H_2O, pyridine*–H_2O, and benzene*–tetracyanoethylene (TCNE) (Fig. 4) was analyzed. These complexes were previously proposed as a suitable test set for excited-state EDA approaches.[35] The asterisk (*) indicates the excited fragment, chosen based on the significantly lower excitation energy, except in the benzene–TCNE system, where the excitation affects both fragments (see Table 1).

In most cases, the excited fragment has excitation energies more than 200 kJ mol^{-1} lower than the other fragment, except for benzene*–TCNE, where benzene's excitation energy is 103 kJ mol^{-1} higher. Despite this, benzene is used as the excited fragment because excitation results in charge transfer from benzene to TCNE (Fig. 8). Thus, only charge transfer systems in which the excited fragment donates electrons to the other fragment are considered. Other types of charge transfer excitations, where the excited fragment acts as an electron acceptor or where ion pairs exist in the ground state and are rebalanced upon excitation, will be examined in future studies. The initial focus here is to establish the fundamental principles of exc-EDA.

All calculations used the TZ2P basis set,[58] numerical quality "VeryGood" and no symmetry. The integration grid was the Becke Grid[59] with quality "VeryGood". No relativistic correction methods were applied, while the exc-EDA is also implemented to be used together with the zeroth order regular approximation (ZORA). As outlined above, no dispersion correction was used.

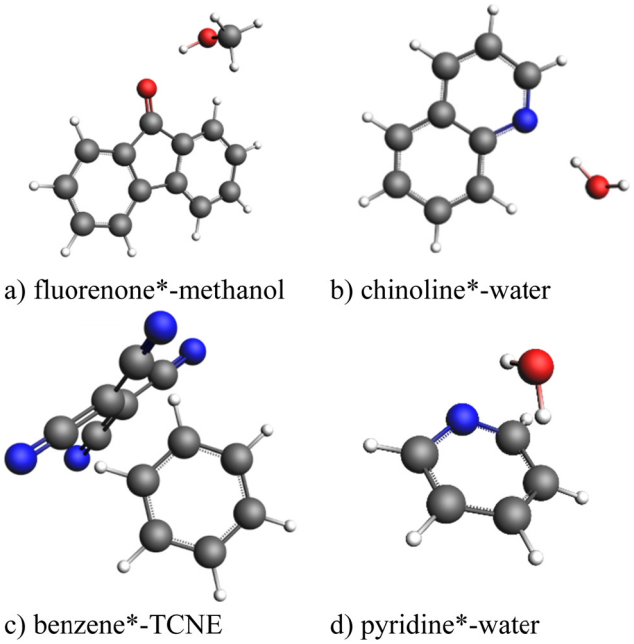

Fig. 4 Test set of exciplexes for exc-EDA. The excited fragment is indicated with an asterisk.

Table 1 Excitation energy for both fragments of the test set of exciplexes[a]

System	Fragment A*	Fragment B
Fluorenone*–methanol	306	624
Quinoline*–water	428	678
Benzene*–TCNE	526	423
Pyridine*–water	461	678

[a] Energies in kJ mol^{-1} with B3LYP/TZ2P without TDA. The asterisk marks the excited fragment A* in exc-EDA.

The structures taken from previous work[35] were reoptimized with B3LYP/TZ2P with the settings outlined above.

Next, exc-EDA was applied to this system, whereby the first singlet excited state was used for both the fragments and the complete systems because it is the most relevant for photochemical processes. These tests were run with and without TDA. For all excitation calculations, the adiabatic local density approximation (ALDA) was applied. Different hybrid functionals (B3LYP,[60] PBE0[61]) and range-separated (hybrid) functionals (CAMY-B3LYP,[62] LC-BLYP,[63] LC-PBE[63]) were used. Previously, it has been shown that the results for the test set for these density functionals are comparable to more accurate EOM-CC data.[35]

Ground state EDA-NOCV and NTO were performed with B3LYP/TZ2P, and settings shown above. The results of these calculations enabled the formulation of expectations regarding the chemical bonding in the excited state. These expectations were then used to rationalize and check the results of the exc-EDA. Thereby, the same setting as the EDA was used.

Furthermore, calculations were conducted using the QCHEM 6.0.0 program package[64] to derive ALMO-EDA results for excited states for the test set. B3LYP was employed as the

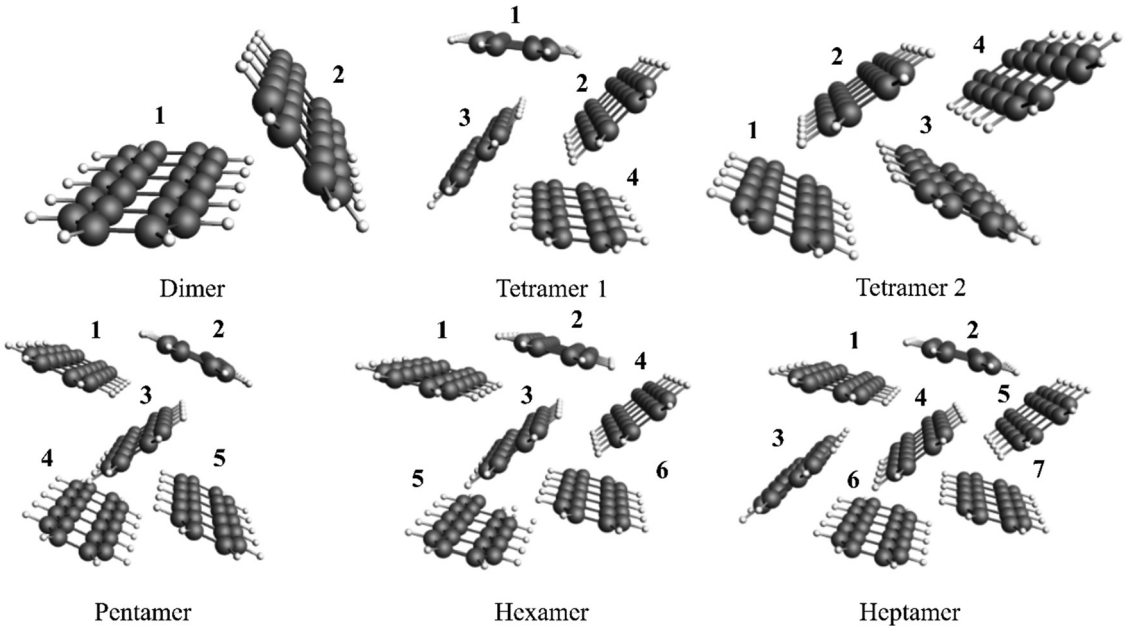

Fig. 5 All considered cluster models of pentacene crystals with numbering.

functional, as it yielded satisfactory outcomes for all functionals with the exc-EDA (see Tables 3, 4, 6 and 7). The def2-QZVPP[65] basis set and the structures from exc-EDA were used for ALMO-EDA. In addition, TDA was employed because the ALMO-EDA is only implemented with TDA. First singlet excitation was calculated for all systems. The SCF convergence criteria were set to 10^{-8} Hartree. Otherwise, the QCHEM default settings were used, and the SG-1 integration grid was applied. No symmetry and no relativistic correction were considered.

Finally, bonding between monomers were analyzed with exc-EDA in pentacene clusters. This system was selected for application of the novel method since it is of interest for singlet fission.[66,67] This will be further discussed below. Engels *et al.*[68] demonstrated that the absorption spectra of pentacene crystals can be replicated with the aid of cluster models using TDDFT. The bonding in different clusters (Fig. 5) was analyzed. Structures were taken from previous work[68] together with the suggested density functional ωB97X-D3[69] and DZP[58] as the basis set, with numerical accuracy set to "normal" for efficiency. The first singlet excitation for the system and the excited fragment were then examined, whereby each monomer is individually considered as an excited fragment in separate exc-EDA calculations.

The tetramer 1 and tetramer 2 reflect different symmetry motives from the solid. In tetramer 1, monomers 1 and 4, as well as monomers 2 and 3, are symmetrically equivalent. In contrast, tetramer 2 has no symmetrically equivalent monomers.

4. Application of exc-EDA

For the systems studied as test set, only the decomposition of the electronic interaction energy is considered. Furthermore, the dispersion contribution in the ground state is also included for pentacene clusters. Consequently, preparation energy (ΔE_{prep}) and bonding energy (ΔE_{bond}) are neither calculated nor discussed, as vertical excitations are considered in this context.

Prior to the analysis of the exc-EDA results, the expected trends based on "chemical intuition" are discussed in the context of each test system. The primary focus is on the EDA contributions of the excitation ω_i (Fig. 2), as these are calculated by exc-EDA. Furthermore, the results obtained with different XC functionals are compared to demonstrate the robustness of the method and to identify potential outliers. A comparison of the results with and without TDA shows that the new method is applicable in both variants.

4.1. Fluorenone–methanol

Fluorenone forms a hydrogen-bond with methanol in the ground state, which is found in ground state EDA (Table 2 for B3LYP and Table S1 (ESI†) for the other density functionals). Here, as for the other systems, we do not see significant changes in the EDA results by using different functionals as was also previously found for a broader test set.[70]

The result for the ground state EDA (Table 2) align with typical hydrogen-bonding interactions, showing an interaction energy between fluorenone and methanol of −26 kJ mol^{-1}. Here, the attractive interactions are primarily governed by $\Delta E^{\text{GS}}_{\text{elstat}}$, which accounts for 2/3 of the total interaction energy, while $\Delta E^{\text{GS}}_{\text{orb}}$ contributes only 1/3. Additionally, the absolute values of Pauli repulsion and electrostatic interaction are comparable.

The first singlet excitation is characterized by a HOMO–LUMO transition,[23,35] with both orbitals localized exclusively on the fluorenone moiety. This makes it an optimal test system. Fig. 6 illustrates the NTO for this excitation, revealing a shift in

Table 2 Ground state EDA results for the test set

	Fluorenone–methanol		Quinoline–water		Benzene–TCNE		Pyridine–water	
$\Delta E_{\text{int}}^{\text{GS}}$	−26		−28		−10		−4	
$\Delta E_{\text{Pauli}}^{\text{GS}}$	41		56		15		21	
$\Delta E_{\text{elstat}}^{\text{GS}}$ [a]	−45	67%	−56	67%	−17	68%	−15	63%
$\Delta E_{\text{orb}}^{\text{GS}}$ [a]	−22	33%	−27	33%	−8	32%	−9	37%

[a] Percentage values give the relative contributions to the attractive EDA terms ΔE_{elstat} and ΔE_{orb}. Energies in kJ mol^{-1}. Computed with B3LYP/TZ2P.

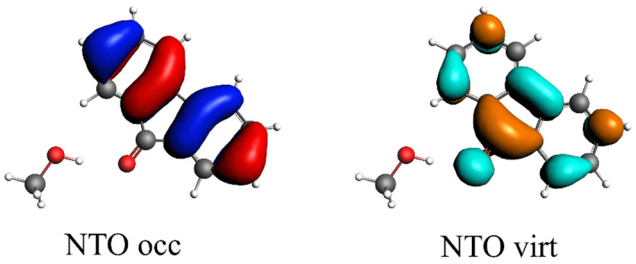

Fig. 6 Calculated NTO of B3LYP/TZ2P/TDA-level for fluorenone–methanol, where the occupied (left) and virtual NTO (right) represent 98% of the density-change for the excitation.

electron density from the π-system of fluorenone towards the oxygen atom. This shift strengthens the hydrogen bond, consistent with the findings of Han *et al.*[71] The increased electron density at the oxygen atom leads to a more pronounced negative charge, suggesting a larger quasi-electrostatic contribution in the excited state. Additionally, the Pauli repulsion is expected to become stronger, as the excitation increases the electron density in the bonding region. Furthermore, the enhanced electron density at the oxygen atom should also result in a greater orbital contribution, given that the orbitals at the oxygen atom play a key role in bonding with methanol.

The results for the excitation contributions ω_i and for the excited state contributions ΔE_i^* of exc-EDA are shown in Table 3.

All results from Table 3 indicate a strengthening of the hydrogen bond, as reflected by the negative value of the interaction contribution ω_{int}. This enhancement is primarily driven by an increase in both ω_{elstat} and ω_{orb}, with ω_{elstat} showing a particularly pronounced effect. Although ω_{Pauli} also increases upon excitation, it remains smaller than the attractive contributions. The EDA contributions ω_i due to the excitation (approximately 25–30%) to the excited state values ΔE_i^* is lower than the contributions of the ground state ΔE_i^{GS}. The only exceptions are some results from range-separated functionals discussed next.

The results indicate only minor functional dependence, with variations smaller than 2 kJ mol^{-1} for all contributions, except for the exc-r-EDA with range-separated functionals. This suggests that the exc-r-EDA variant significantly overestimates ω_{elstat}, which is counterbalanced by the large values for ω_{Pauli}. This discrepancy arises because the intermediate states involve different excited states, corresponding to excitations from lower occupied MOs (HOMO−10 and HOMO−9) to LUMO and LUMO+1. As a result, these findings can be considered outliers.

The outcomes of the fluorenone–methanol system demonstrate minimal difference (less than 1 kJ mol^{-1}) between the calculations with and without TDA except for the discussed outliers. For the exc-r-EDA the change of using TDA is 7 kJ mol^{-1} (7%) for CAM-B3LYP and 9 kJ mol^{-1} (3%) for both others, while this does not change the character of the bond. Therefore, TDA provides a satisfactory approximation for the system as it was found for TDDFT in general.[55]

Table 3 Results of exc-EDA for fluorenone–methanol[a]

	Without TDA					TDA				
Exc-u-EDA	PBE0	B3LYP	CAMY-B3LYP	LC-BLYP	LC-PBE	PBE0	B3LYP	CAMY-B3LYP	LC-BLYP	LC-PBE
ω_{int}	−12	−12	−12	−13	−13	−12	−12	−13	−13	−13
ω_{Pauli}	12	13	13	13	13	13	13	13	12	12
ω_{elstat}	−15	−15	−15	−14	−14	−16	−16	−16	−15	−15
ω_{orb}	−9	−9	−10	−11	−11	−9	−9	−10	−11	−10
ΔE_{int}^*	−41	−38	−44	−51	−46	−41	−38	−44	−51	−46
$\Delta E_{\text{Pauli}}^*$	49	54	48	42	45	49	54	48	41	44
$\Delta E_{\text{elstat}}^*$	−59	−60	−61	−62	−60	−60	−61	−61	−62	−60
ΔE_{orb}^*	−30	−31	−31	−31	−31	−30	−31	−31	−30	−30
Exc-r-EDA	PBE0	B3LYP	CAMY-B3LYP	LC-BLYP	LC-PBE	PBE0	B3LYP	CAMY-B3LYP	LC-BLYP	LC-PBE
ω_{int}	−12	−12	−12	−13	−13	−12	−12	−13	−13	−13
ω_{Pauli}	13	13	93	264	232	13	13	100	273	241
ω_{elstat}	−17	−17	−96	−267	−235	−16	−16	−103	−276	−244
ω_{orb}	−8	−8	−9	−10	−10	−9	−9	−9	−10	−10
ΔE_{int}^*	−41	−38	−44	−51	−46	−41	−38	−44	−51	−46
$\Delta E_{\text{Pauli}}^*$	49	54	128	293	264	49	54	135	302	273
$\Delta E_{\text{elstat}}^*$	−60	−62	−142	−314	−281	−60	−61	−149	−323	−290
ΔE_{orb}^*	−29	−30	−30	−30	−29	−30	−31	−31	−30	−30

[a] Energies in kJ mol^{-1} with TZ2P.

The results from exc-EDA can be rationalized by the increase in electron density at the oxygen atom of fluorenone upon excitation, as hypothesized in the beginning of the section. The strength of exc-EDA lies in its ability to quantitatively compare such effects across different systems.

4.2. Quinoline–water

As in the previous system, a hydrogen bond forms between the heteroatom in the aromatic ring of quinoline and water in the ground state. The ground state EDA results for this interaction are presented in Table 2 for B3LYP and in Table S2 (ESI†) for the other density functionals. The attractive interaction is again dominated by electrostatic interactions (63%) and also here, the Pauli repulsion has similar value than the electrostatic contribution.

The NTOs for the first singlet state of the system (Fig. 7) show that the excitation occurs exclusively within the π-system of quinoline. Unlike the previous system, this excitation includes contributions from both the HOMO → LUMO and HOMO−1 → LUMO+1 transitions.[23,35] Since all these orbitals are part of the π-system of quinoline, only quinoline needs to be considered as excited fragment A*. Additionally, Fig. 7 shows a slight increase in electron density at the nitrogen atom. Unlike the previous system, nitrogen orbitals are involved in both the occupied and virtual NTOs, with a slightly higher proportion for the virtual NTOs. Given the smaller increase in electron density on nitrogen compared to the previous system, we expect similar effects (stronger electrostatic interactions, Pauli repulsion, and orbital interactions) but to a lesser degree.

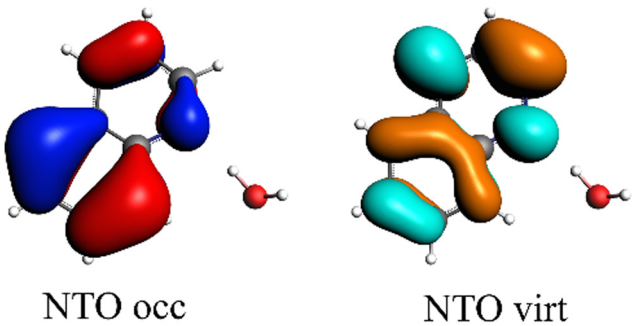

Fig. 7 Calculated NTO (B3LYP/TZ2P/TDA) for quinoline–water, where the occupied (left) and virtual NTO (right) represent 90% of the excitation.

The results of the EDA analysis for the quinoline–water system are presented in Table 4.

For this system, the results differ significantly between calculations with and without TDA, except for LC-BLYP. As anticipated, the calculation without TDA shows a slight strengthening of ω_{int} (less pronounced than in the fluorenone–methanol system). Conversely, when TDA is applied, the bond is weakened, except for LC-BLYP. This discrepancy can be attributed to the different excited states computed with and without TDA, as illustrated in Table 5.

The data in Table 5 show that the excitation without TDA for the fragment and the full system are similar, with discrepancies of less than 2% in the orbital contributions, leading to comparable bond stabilization. For both the system and the fragment, the excitation is predominantly a HOMO → LUMO transition, accounting for approximately 90% of the total excitation. Additionally, HOMO−1 → LUMO+1 excitations contribute with values of 5% and 3% for the fragment and system, respectively, as calculated with CAM-B3LYP, and about 10% for the LC functionals. In calculations with TDA, except for LC-BLYP, there is a marked divergence between the excitation character of the fragment and the system, with contribution changes exceeding 10%. For LC-BLYP, the excitation is comprised of 60% HOMO−1 → LUMO and 35% HOMO → LUMO+1 transitions. This divergence highlights significant differences between

Table 4 Results of exc-EDA for quinoline–water[a]

	Without TDA					TDA				
Exc-u-EDA	PBE0	B3LYP	CAMY-B3LYP	LC-BLYP	LC-PBE	PBE0	B3LYP	CAMY-B3LYP	LC-BLYP	LC-PBE
ω_{int}	−9	−9	−8	−5	−5	27	26	19	−1	8
ω_{Pauli}	12	11	12	13	13	−17	−17	−21	6	−23
ω_{elstat}	−5	−5	−5	−5	−5	82	81	88	−2	92
ω_{orb}	−15	−16	−15	−14	−14	−38	−39	−48	−5	−61
ΔE^*_{int}	−41	−37	−41	−45	−42	−4	−2	−14	−41	−29
ΔE^*_{Pauli}	62	67	62	58	59	33	39	29	51	23
ΔE^*_{elstat}	−60	−61	−62	−64	−62	27	25	31	−61	35
ΔE^*_{orb}	−42	−44	−42	−39	−39	−65	−66	−74	−31	−86
Exc-r-EDA	PBE0	B3LYP	CAMY-B3LYP	LC-BLYP	LC-PBE	PBE0	B3LYP	CAMY-B3LYP	LC-BLYP	LC-PBE
ω_{int}	−9	−9	−8	−5	−5	27	26	19	−1	8
ω_{Pauli}	138	139	229	374	338	147	149	228	360	325
ω_{elstat}	−134	−134	−224	−368	−333	−110	−113	−206	−357	−312
ω_{orb}	−13	−14	−12	−10	−10	−10	−10	−3	−4	−4
ΔE^*_{int}	−41	−37	−41	−45	−42	−4	−2	−14	−41	−29
ΔE^*_{Pauli}	188	194	279	418	383	197	204	278	405	371
ΔE^*_{elstat}	−189	−191	−281	−427	−390	−165	−169	−263	−416	−370
ΔE^*_{orb}	−40	−41	−39	−35	−35	−37	−37	−30	−29	−29

[a] Energies in kJ mol^{-1} with TZ2P.

Table 5 All contributions of a single orbital transition with >5% of quinoline and quinoline–H_2O excitation with and without TDA and TZ2P basis set

	Without TDA		With TDA	
	Quinoline	Quinoline–H_2O	Quinoline	Quinoline–H_2O
B3LYP	93% HOMO → LUMO	93% HOMO → LUMO	98% HOMO1 → LUMO1	83% HOMO → LUMO 5% HOMO1 → LUMO1
PBE0	93% HOMO → LUMO	94% HOMO → LUMO	98% HOMO2 → LUMO	88% HOMO2 → LUMO 7% HOMO3 → LUMO
CAM-B3LYP	93% HOMO → LUMO 5% HOMO1 → LUMO1	94% HOMO → LUMO	95% HOMO2 → LUMO	56% HOMO1 → LUMO 38% HOMO → LUMO1
LC-BLYP	87% HOMO → LUMO 11% HOMO1 → LUMO1	89% HOMO → LUMO 9% HOMO1 → LUMO1	58% HOMO1 → LUMO 37% HOMO → LUMO1	60% HOMO1 → LUMO 36% HOMO → LUMO1
LC-PBE	87% HOMO → LUMO 10% HOMO1 → LUMO1	89% HOMO → LUMO 10% HOMO1 → LUMO1	87% HOMO2 → LUMO 7% HOMO2 → LUMO3	59% HOMO1 → LUMO 37% HOMO → LUMO1

functionals, and the lack of similar excitations across functionals complicates the reconciliation of exc-EDA results with TDA. Consequently, we focus on results obtained without TDA for this system. To avoid such issues, it is advisable to benchmark the appropriateness of TDA for the system and fragment under investigation.

In addition to strengthening the bond, all contributions increase upon excitation (without TDA). The results for different variants of exc-EDA show relatively large differences, reflecting their inherent properties. The exc-r-EDA results reveal that the values for ω_{elstat} and ω_{Pauli} are overestimated. Specifically, these values exceed 130 kJ mol^{-1} for hybrid functionals and are over 220 kJ mol^{-1} and more than 330 kJ mol^{-1} for CAM-B3LYP and LC functionals, respectively. This is due to the different excited states involved in the intermediate steps, as indicated by the results with TDA, which show multiple close-lying excitations.

For exc-u-EDA, the deviations of all contributions between functionals are less than 4 kJ mol^{-1}, with all contributions being approximately 10 kJ mol^{-1}. The bond strengthening primarily arises from ω_{bond}, which increases three times more than ω_{orb}. The increase in ω_{Pauli} is 1 kJ mol^{-1} less for LC compared to ω_{orb} and 3 kJ mol^{-1} less for the other functionals. The largest contribution to the bonding comes from the ground state interactions. Specifically, the excitation contribution to the electrostatic interaction is minimal, at approximately 8% of the total, whereas the excitation contributions are 35% for the orbital term and between 16% and 22% for Pauli repulsion.

In general, the outcomes of exc-u-EDA without TDA support the hypothesis that the bond is more readily strengthened compared to the fluorenone system, owing to a more pronounced increase in electron density at the heteroatom. However, the remaining results are complicated by the presence of multiple close-lying excited states.

4.3. Benzene–TCNE

In the ground state the bond between benzene and TCNE is weaker as in the previous systems and the ground state EDA results are represented in Table 2 for B3LYP and the other functional in Table S3 (ESI†). It shows a similar relative contribution of electrostatic (68%) to orbital (32%) terms to the attractive interaction. Additionally, the Pauli repulsion is observed to be of slightly smaller value than the electrostatic contribution.

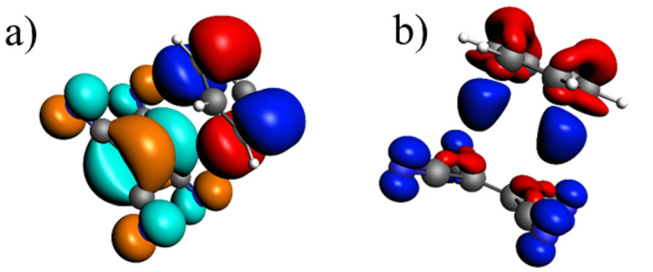

Fig. 8 (a) Calculated NTO (B3LYP/TZ2P/TDA) for benzene–TCNE, whereby the occupied (red and blue) and virtual NTO (orange and green) make up 99% of the excitation; (b) the most important deformation density (B3LYP/TZ2P, charge flow from red to blue) which makes up 36% of the total orbital interaction.

To gain a deeper understanding of the orbital interactions and the processes occurring during excitation, NOCVs were also calculated. The inclusion of NOCVs was necessary because NTOs alone (Fig. 8a) are insufficient for estimating the EDA contributions in the excited state due to a significant charge transfer (CT) character of the excitation. The most significant NOCV-based deformation density is depicted in Fig. 8b (further NOCV data are found in the ESI,† Fig. S1) which shows the charge transfer from the π-system of benzene to the antibonding π-orbitals of TCNE. Fig. 8a displays the first singlet excitation for the system *via* NTO, which confirms it as a charge transfer excitation.[35,72] As with the NOCVs, the electron density shifts from the π-system of benzene to the antibonding π-orbitals of TCNE. Unlike the previous system, both fragments are involved in the excitation. Since only electrons from benzene orbitals are excited, fragmentation of the excitation is possible and thus the exc-EDA can be used. Therefore, the bonding analysis can be conducted by focusing only on the excitation of benzene as the fragment. Thus, the excitation of this compound is considered in such a way that first the benzene moiety is excited and then in a second step interacts with TCNE leading to CT.

The Pauli repulsion is not expected to change significantly due to excitation, as the charge density in the bonding regions remains relatively constant. The excitation results in charge

Table 6 Results of exc-EDA for benzene–TCNE[a]

	Without TDA					TDA				
Exc-u-EDA	PBE0	B3LYP	CAMY-B3LYP	LC-BLYP	LC-PBE	PBE0	B3LYP	CAMY-B3LYP	LC-BLYP	LC-PBE
ω_{int}	−329	−339	−281	−223	−226	−331	−341	−284	−173	−175
ω_{Pauli}	182	179	199	213	204	174	173	184	206	198
ω_{elstat}	2	2	2	0	0	1	2	1	0	0
ω_{orb}	−512	−519	−481	−436	−430	−506	−516	−469	−379	−373
ΔE^*_{int}	−345	−348	−297	−247	−247	−347	−350	−300	−197	−196
ΔE^*_{Pauli}	190	194	207	215	209	182	188	193	208	203
ΔE^*_{elstat}	−15	−15	−16	−19	−18	−15	−15	−16	−19	−18
ΔE^*_{orb}	−520	−527	−488	−443	−438	−514	−523	−476	−386	−380
Exc-r-EDA	PBE0	B3LYP	CAMY-B3LYP	LC-BLYP	LC-PBE	PBE0	B3LYP	CAMY-B3LYP	LC-BLYP	LC-PBE
ω_{int}	−329	−339	−281	−223	−226	−331	−341	−284	−173	−175
ω_{Pauli}	103	101	113	144	136	103	101	112	143	136
ω_{elstat}	−334	−344	−285	−235	−236	−336	−347	−289	−185	−184
ω_{orb}	−98	−95	−108	−132	−126	−97	−95	−107	−131	−126
ΔE^*_{int}	−345	−348	−297	−247	−247	−347	−350	−300	−197	−196
ΔE^*_{Pauli}	110	116	121	146	141	110	115	121	146	141
ΔE^*_{elstat}	−350	−361	−303	−254	−254	−353	−363	−306	−204	−202
ΔE^*_{orb}	−105	−103	−115	−139	−134	−105	−103	−115	−139	−134

[a] Energies in kJ mol^{-1} with TZ2P.

transfer, which leads to the formation of differently charged fragments within the system, likely increasing the electrostatic contribution. However, since this charge transfer is the primary contributor to the orbital interaction, it is anticipated that the orbital contribution will be reduced, as the charge transfer has already occurred. This picture is only expected for the exc-r-EDA variant since the exc-u-EDA variant considers all charge transfer in the orbital contribution. Thus, for this variant, the stabilization should be mainly due to an increase in the orbital contribution. The results of the bonding analysis are shown in Table 6.

Overall, the benzene–TCNE system exhibits the greatest strengthening of the bonding due to excitation, with values ranging from −180 to −340 kJ mol^{-1} for ω_{int}. Hybrid functionals show the largest increase, around −330 kJ mol^{-1}, followed by CAM-B3LYP at approximately −280 kJ mol^{-1}. Long-range corrected functionals display the smallest values of about −220 kJ mol^{-1} and −180 kJ mol^{-1}. This significant increase can primarily be attributed to charge transfer from benzene to TCNE.

As expected, the results of the two variants of exc-EDA differ substantially for this system. The results with and without TDA are relatively similar for both variants, with discrepancies of less than 8% for exc-u-EDA and less than 1% for exc-r-EDA. Importantly, these variations do not alter the character of the bond. However, there are two notable exceptions. First, for long-range corrected functionals, the difference is approximately 20% for ω_{int} and 12% for ω_{orb} with exc-u-EDA, and 20% for ω_{elstat} with exc-r-EDA. This discrepancy in ω_{int} is also observed with exc-r-EDA, as both variants yield comparable interaction energies. Overall, the differences fall within the expected range for using TDA. Second, ω_{elstat} is near zero for exc-u-EDA while it is substantial for exc-r-EDA. This was anticipated since the exc-u-EDA variant encounters difficulties in describing this system because all effects of the charge transfer are encapsulated in ω_{orb}. This also explains the relatively large value for ω_{orb}, exceeding 400 kJ mol^{-1}. Additionally, ω_{Pauli} increases by approximately 200 kJ mol^{-1}. For hybrid functionals, the increase of ω_{Pauli} due to excitation is about 30 kJ mol^{-1} smaller than for long-range corrected functionals, while the gain in ω_{orb} is 80 kJ mol^{-1} larger, leading to differences in ω_{int}. The results for CAM-B3LYP fall between these two extremes. Conversely, the results from the exc-r-EDA variant indicate that the significant strengthening of the bond is primarily attributed to the enhancement of ω_{elstat}, which is 2–3 times larger than the increase in ω_{orb}, consistent with expectations. However, contrary to expectations, there is also a notable increase in ω_{Pauli}. This suggests that the electron density in the bonding plane is slightly augmented by the excitation. The strengthening of both ω_{Pauli} and ω_{orb} is 40 kJ mol^{-1} greater for LC functionals compared to hybrid functionals. Conversely, the gain in electrostatic attraction is approximately 100 kJ mol^{-1} smaller for LC functionals. This discrepancy can be attributed to the superior description of the exchange contributions, which more comprehensively accounts for long-range interactions between orbitals. As a result, the proportion of the attractive interaction from the orbital contribution increases from 23% (in hybrids) to 35% (in LC functionals). As with the other variant, the results for CAM-B3LYP fall between these extremes.

Notably, both exc-EDA variants exhibit greater functional dependence here compared to previous test systems. This is not a result of the method itself but rather stems from the TDDFT calculation of the excited state. The behavior of the EDA contributions mirrors that of the interaction energy, which is calculated independently of the EDA method. Notably, all EDA contributions in the excited state are primarily influenced by the changes induced by the excitation (over 90%), given the relatively small values in the ground state.

Moreover, this system highlights the usefulness of the exc-r-EDA variant, as it is the only variant capable of producing results for CT excitations that align with bonding considerations. Therefore, a difference between the two variants is an indicator for a CT excitation.

4.4. Pyridine–water

The bond between the π-system of pyridine and water is analogous to the bond in the preceding system, though it exhibits a slightly weaker interaction, with a bonding energy of 5 kJ mol^{-1}. This similarity is reflected in the EDA results, which are presented in Table 2 for B3LYP and in Table S4 (ESI†) for the other functionals.

The attractive interaction is predominantly driven by electrostatic interactions, which accounts for approximately 63% of the total interaction energy. This stems from the electron density of the π-system in the aromatic ring interacting with the positively charged hydrogen atom of the water molecule, a contribution slightly smaller than that observed in the benzene–TCNE system. The Pauli repulsion (21 kJ mol^{-1}) is the largest contribution, exceeding the electrostatic component by 6 kJ mol^{-1}. This higher Pauli repulsion accounts for the relatively low overall interaction energy.

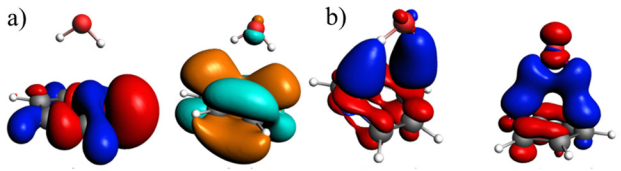

Fig. 9 (a) Calculated NTO (B3LYP/TZ2P/TDA) for pyridine–water, whereby the occupied (red and blue) and virtual NTO (orange and green) make up 99% of the excitation; (b) two important deformation densities (B3LYP/TZ2P, charge transfer from red to blue), which represent 38% (left) and 24% (right) of the total orbital interaction energy.

As with the previous system, NOCVs were calculated to gain deeper insights into the orbital interactions. The two most significant deformation densities for the ground state, along with the NTO, are shown in Fig. 9 (additional data in Fig. S4, ESI†). The most significant NOCVs primarily reveal a charge transfer from the π-system of pyridine to the bonding plane, specifically into the antibonding orbitals of water. Examination of the NTO reveals that the electron density originating from the π-system is transferred into an NTO that closely resembles NOCV 2. The virtual NTO also includes portions of the water orbitals. However, since the occupied NTO is localized on pyridine, the fragmentation can be effectively modeled by exciting only the pyridine in the fragment calculations.

The orbital contribution is significantly enhanced by the excitation, as the interaction described by NOCV 2 (Fig. 9b, right) is strengthened due to the increased electron density. This increased electron density in the bonding plane leads to an increase in Pauli repulsion. Additionally, the excitation slightly reduces the electron density in the π-system, weakening the interaction with the positively charged hydrogen atom. Simultaneously, the excitation enhances the electrostatic interaction through a minor charge transfer from pyridine to water. Overall, the electrostatic interaction is expected to be slightly increased by the excitation. The exc-EDA results of the final test system, pyridine–water, are presented in Table 7.

The results presented in Table 7 show an increase in all EDA contributions. Notably, the enhancement of ω_{orb} exceeds that of ω_{elstat}, except in the case of exc-r-EDA with range-separated functionals. However, the more substantial increase in the attractive contributions is offset by an even greater increase in ω_{Pauli}, leading to a modest overall bond enhancement of 5 kJ mol^{-1} across all calculations.

Table 7 Results of exc-EDA for pyridine–water[a]

	Without TDA					TDA				
Unrelaxed	PBE0	B3LYP	CAMY-B3LYP	LC-BLYP	LC-PBE	PBE0	B3LYP	CAMY-B3LYP	LC-BLYP	LC-PBE
ω_{int}	−5	−5	−5	−5	−5	−5	−5	−5	−5	−5
ω_{Pauli}	145	148	162	205	172	162	164	181	228	192
ω_{elstat}	−9	−9	−11	−14	−13	−10	−10	−12	−16	−14
ω_{orb}	−141	−144	−157	−195	−164	−156	−160	−174	−217	−182
ΔE^*_{int}	−14	−9	−14	−20	−18	−14	−9	−14	−20	−17
ΔE^*_{Pauli}	161	168	177	214	183	177	185	196	238	203
ΔE^*_{elstat}	−24	−24	−26	−31	−29	−25	−25	−28	−32	−30
ΔE^*_{orb}	−150	−153	−165	−203	−172	−165	−169	−183	−225	−191
Relaxed	PBE0	B3LYP	CAMY-B3LYP	LC-BLYP	LC-PBE	PBE0	B3LYP	CAMY-B3LYP	LC-BLYP	LC-PBE
ω_{int}	−5	−5	−5	−5	−5	−5	−5	−5	−5	−5
ω_{Pauli}	274	280	401	865	1265	278	284	401	589	551
ω_{elstat}	−121	−125	−227	−653	−1060	−127	−130	−232	−383	−350
ω_{orb}	−157	−161	−180	−217	−211	−156	−159	−174	−211	−205
ΔE^*_{int}	−14	−9	−14	−20	−18	−14	−9	−14	−20	−17
ΔE^*_{Pauli}	289	301	417	875	1277	293	305	416	599	562
ΔE^*_{elstat}	−137	−140	−242	−669	−1076	−142	−145	−247	−400	−366
ΔE^*_{orb}	−166	−170	−189	−225	−219	−165	−169	−183	−219	−213

[a] Energies in kJ mol^{-1} with TZ2P.

When applying the TDA, the exc-u-EDA contributions become 10% more negative. Except for ω_{elstat} and ω_{Pauli} with LC-functionals, the deviation due to TDA remains under 5%. However, the difference between these contributions and others is significantly larger (exceeding 30%) suggesting an artificial alteration in the excitation for the intermediate states. Despite these deviations, the overall character of the bond remains unchanged. The two exc-EDA variants lead to different results due to the partial CT nature of the excitation. Particularly noticeable are deviations in the ω_{Pauli} and the ω_{elstat} contributions, with differences of over 100 kJ mol^{-1}. The ω_{elstat} term of exc-u-EDA is about 10 kJ mol^{-1}, which is significantly higher than in previous systems. ω_{Pauli} and ω_{orb} contributions are similar, but significantly larger than ω_{elstat}, with ω_{Pauli} increasing by 5–10 kJ mol^{-1} more than ω_{orb}. For the hybrid functionals, ω_{Pauli} and ω_{orb} are smaller about 15–20 kJ mol^{-1} compared to CAMY-B3LYP and LC-PBE0, while LC-BLYP shows an increase of about 30 kJ mol^{-1}. Nevertheless, the character of the bond remains unchanged.

For exc-r-EDA, the increase in the electrostatic contribution is larger than 100 kJ mol^{-1}. For the hybrid functionals, ω_{elstat} accounts for about 55% of the attractive interactions. For CAMY-B3LYP the electrostatic contribution is 57%, for the long-range corrected functionals even 65–85%. ω_{orb} is similar for exc-r-EDA as for exc-u-EDA, but the ω_{Pauli} are significantly larger for exc-r-EDA to compensate for the larger increase in attractive interactions. For hybrid functionals, ω_{Pauli} is about 120 kJ mol^{-1} lower for exc-r-EDA than for CAMY-B3LYP and over 270 kJ mol^{-1} lower for long-range corrected functionals. All EDA contributions increase by a total of 88%, while the excitation contribution accounts for less than half of the total interaction energy for the excited state.

The findings indicate that the formation of charged fragments due to CT also enhances the electrostatic contribution. This partial CT character is evident when comparing the two variants. Unlike the benzene–TCNE bond, the stabilization of the bond here is more significantly influenced by the strengthening of orbital interactions. However, the substantial increase in attractive interactions is almost completely offset by a concurrent rise in Pauli repulsion due to the increased electron density in the bonding plane.

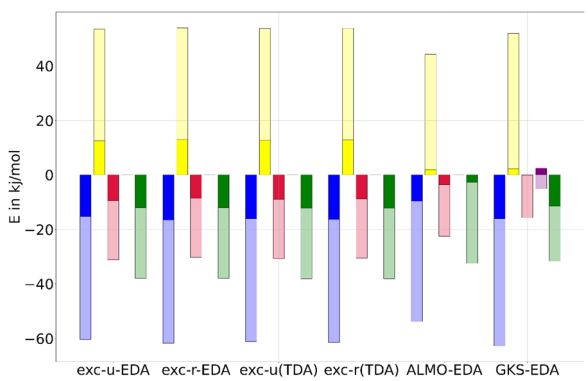

Fig. 10 Comparing exc-EDA (both variants, with and without TDA), ALMO-EDA, and GKS-EDA for the first singlet excitation of the fluorenone–methanol exciplex. Shown are the electrostatic (blue), Pauli repulsion (yellow), the orbital term (red), and interaction (green). Additionally, the correlation contribution (purple) is presented for GKS-EDA. The more intense colored bar represents the change in the respective contribution resulting from excitation, while the total (including the paler portion) bars indicate the value of the contribution for the excited state.

4.5. Comparison with ALMO-EDA and GKS-EDA

For comparison with ALMO-EDA and GKS-EDA, we focus on the B3LYP results, which offer reasonable outcomes both with and without TDA, as discussed in previous sections. Thereby the GKS-EDA were taken from ref. 35. In ALMO-EDA, the charge transfer ΔE_{CT} and polarization contributions ΔE_{POL} are combined into an orbital contribution ΔE_{orb}, facilitating a more meaningful comparison with exc-EDA. In this context, the electrostatic term $\Delta E_{CLS_{ELEC}}$ in ALMO-EDA corresponds to the quasi-electrostatic contribution ΔE_{elstat}, while the Pauli term ΔE_{Pauli} aligns with Pauli repulsion ΔE_{Pauli}. In GKS-EDA, the electrostatic term ΔE^{ele} is analogous to the quasi-electrostatic contribution ΔE_{elstat}, the exchange-repulsion term ΔE^{exrep} corresponds to Pauli repulsion ΔE_{Pauli}, and the polarization term ΔE^{pol} relates to the orbital contribution ΔE_{orb} for this comparison. The correlation contribution ΔE^{cor} in GKS-EDA cannot be directly attributed to any component of exc-EDA, as it reflects the difference in XC energy and exact exchange between the system and the fragment.

ALMO-EDA is applicable only within the framework of TDDFT with TDA, whereas the GKS-EDA results were computed without TDA are taken from ref. 35. The comparison of results is illustrated in Fig. 10 for the fluorenone–methanol system and detailed in Table S5 (ESI†). The excited state EDA values are dominated by the ground state contributions, which are then modestly enhanced by the excitation. An exception to this trend is observed in the GKS-EDA results, where the polarization contribution shows negligible change (less than 1 kJ mol^{-1}), and a weakening of the ground state effect is noted for the correlation contribution. For the hydrogen bond between fluorenone and methanol, the bond strengthening due to excitation is predominantly attributed to the enhancement of the electrostatic interaction across all methods. Additionally, both ALMO-EDA and exc-EDA methods show a significant increase in orbital contribution. Despite this similarity, ALMO-EDA reports generally smaller contributions compared to exc-EDA, with a notable difference in the excitation effects and especially in the Pauli repulsion. Specifically, exc-EDA shows an increase in Pauli repulsion due to excitation that is approximately ten times greater than that observed with ALMO-EDA.

It is important to emphasize that while the absolute values of these contributions are informative, the relative magnitudes are more critical, as all EDA methods rely on comparison of trends between systems. The comparison for the fluorenone–methanol bond indicates that exc-EDA provides similar conclusions than previously published analysis methods.

4.6. Pentacene clusters

Finally, exc-EDA was applied to analyze pentacene molecular crystals in a cluster approximation. Singlet fission processes

could be demonstrated for pentacene crystals,[66,67] indicating it to be an interesting system for organic semiconductors and solar cells. The advantage of singlet fission lies in the spin-allowed generation of two triplet states, which facilitates charge separation while significantly hindering charge recombination due to this being a spin-forbidden process. Additionally, the Engels group demonstrated that the high-resolution experimental absorption spectra of thin films of pentacene can be reproduced with TDDFT calculations using a cluster approach.[68] Consequently, exc-EDA will be employed to examine pentacene clusters. The objective of the investigation is to ascertain how the bonding between an excited pentacene and the surrounding pentacene molecules in the ground state varies with an increasing number of monomers in the cluster model. This state represents the first step of singlet fission. Consequently, the potential driving forces for this process can be identified. Additionally, the number of monomers involved in or influencing the excitation through CT effects can be examined, as shown above for the benzene–TCNE system. In this process, one monomer is initially excited, and the subsequent interaction with other monomers occurs *via* CT.

The results of the exc-EDA calculations are shown in Fig. 11. For each cluster, sequential exc-EDA calculations were carried out, exciting one pentacene monomer at a time. Afterwards, these results were averaged.

Fig. 11 illustrates that bonding interactions in all clusters are predominantly governed by ground state contributions, with only modest changes due to excitation. The primary exception is Pauli repulsion, which shows minimal ground state contributions and a relatively pronounced change due to excitation. For exc-u-EDA, the orbital contribution in the excited state is evenly split between ground and excitation contributions. In the ground state, the electrostatic interaction exceeds the orbital interaction by approximately 30%, with this difference increasing as the cluster size grows. This trend is consistent with the long-range nature of the electrostatic interaction. The dispersion interactions determined only in the ground state are of comparable magnitude to the electrostatic contribution for all clusters. Additionally, Pauli repulsion remains very small, less than 20 kJ mol^{-1}, or about 10% of the electrostatic interaction.

As the size of the cluster model increases, the strength of the interactions also increases. However, the results for the pentamer are anomalous, showing interaction strengths similar to those of tetramer 2 and smaller than those of tetramer 1. Despite this anomaly, the effect on the overall bonding character remains consistent across different clusters. Furthermore, there is no noticeable convergence in interaction energies up to the heptamer, with a difference of 40 kJ mol^{-1} observed between the hexamer and heptamer. This suggests the presence of long-range effects, indicating that additional molecules may be necessary to accurately simulate the bonding.

Fig. 11 also shows the changes in EDA contributions due to the initial excitation, highlighting the occurrence of CT.

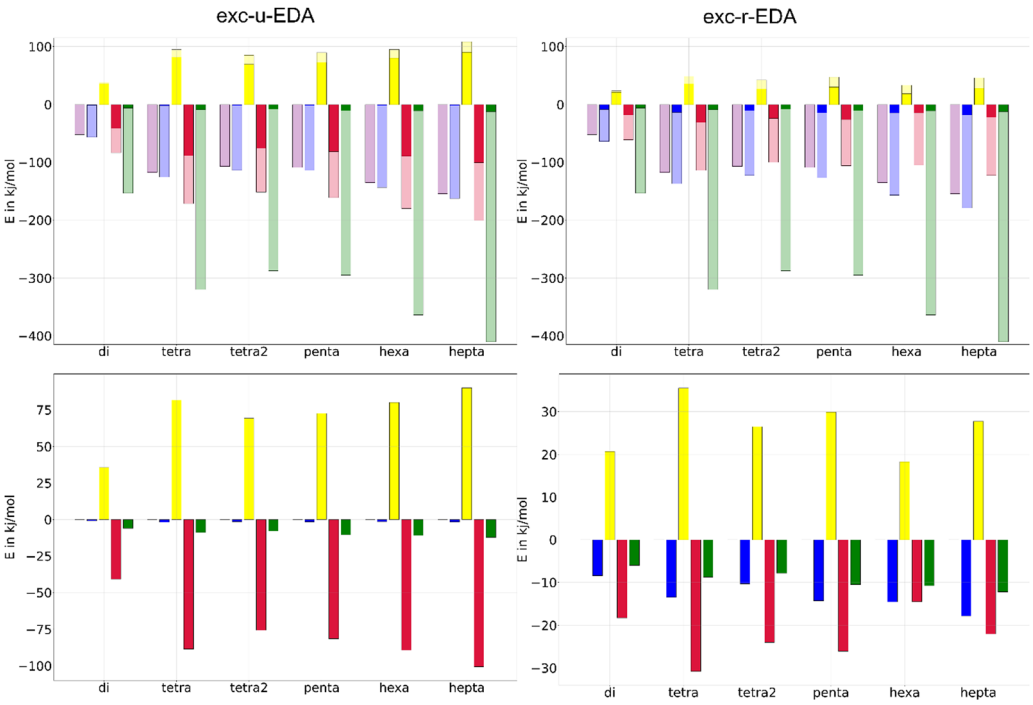

Fig. 11 Averaged exc-EDA values on ωB97X-D3/DZP-level over the different excited fragments for the first singlet excitation of the different cluster models. Shown are the electrostatic (blue), Pauli repulsion (yellow), the orbital term (red), and interaction energy (green). Additionally, the dispersion contribution (purple) is presented for the ground state. The more intense colored bar represents the change in the respective contribution resulting from excitation, while the total (including the paler portion) bars indicate the value of the contribution for the excited state. The exc-u-EDA results are on the left side and the exc-r-EDA results are on the right side. The bottom two are zoomed in on the EDA results for the excitation contribution.

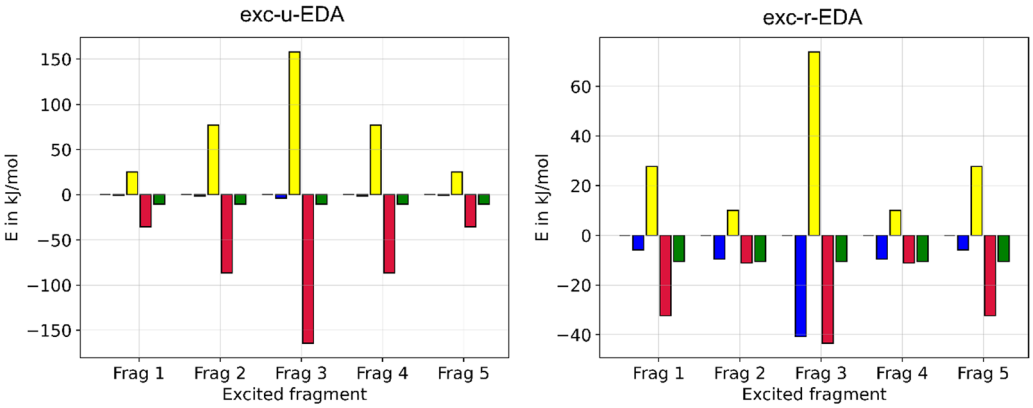

Fig. 12 Exc-EDA excitation values (ωB97X-D3/DZP) for the first singlet excitation of pentacene pentamer, where different monomers are excited. Shown is the electrostatic (blue), Pauli repulsion (yellow), the orbital term (red), and interaction (green).

The negligible values of the electrostatic component observed in the exc-u-EDA results are indicative of this CT. In contrast, the exc-u-EDA results demonstrate a significant amplification of the orbital term compared to the exc-r-EDA results. This observation aligns with findings by Guldi *et al.*[73,74] who reported that in pentacene dimers with weak coupling through a molecular linker, the excitation of one monomer leads to charge transfer to the other monomers. The exc-u-EDA analysis results show that the relative change in EDA contributions is consistent across all cluster structures due to excitation. The primary factor in this consistency is the substantial enhancement of orbital interactions, which contributes over 98% to the overall increase in attractive interactions. In contrast, the electrostatic contribution shows only a minor increase of 2 kJ mol^{-1}. The larger enhancement in orbital interactions is balanced by a corresponding increase in Pauli repulsion, whereby this increase is approximately 10 kJ mol^{-1} smaller than by orbital interaction. As a result, the net strengthening of interactions amounts to about 10 kJ mol^{-1}. For dimers, the enhancements are notably smaller compared to other clusters, with a 40 kJ mol^{-1} difference in Pauli repulsion and orbital contributions, while the interaction energy difference is only 2 kJ mol^{-1}. The results for larger clusters are similar, differing by less than 15 kJ mol^{-1}, except for the pentacene heptamer, which shows a 10 kJ mol^{-1} larger gain.

In comparison to the exc-u-EDA, the alteration in ω_{Pauli} and ω_{orb} is smaller by 50% for exc-r-EDA. This is because CT excitation is decomposed by the exc-r-EDA. Exc-r-EDA amplifies all EDA contributions due to excitation, with the most significant increase observed in ω_{Pauli} across all clusters. ω_{orb} is around 20 kJ mol^{-1}, with a range from 15 kJ mol^{-1} for the hexamer to 31 kJ mol^{-1} for the tetramer. In contrast to exc-u-EDA, additional increase of the electrostatic term is found due to the generation of charged fragments by CT, with this effect increasing with cluster size. For smaller clusters, the increase in the orbital term is about 70% due to excitation. ω_{elstat} and ω_{orb} are approximately similar for hexamers and heptamers. Therefore, for exc-r-EDA to yield results comparable to the largest cluster, a hexamer is necessary. Only from the tetramers onwards the difference is already significantly smaller. This aligns with Engels' findings, which suggest that a tetramer suffices for accurate absorption spectra predictions with exc-u-EDA.

Finally, we investigated the influence of different monomers on the exc-EDA contributions. Results for the pentamer are shown in Fig. 12.

Fig. 12 illustrates that the change in interaction energy due to excitation is qualitatively independent of which monomer is excited. This is because the energy difference between the pentamer and a monomer's excitation is relatively constant, regardless of fragmentation. Further, symmetry equivalent monomers yield similar results. The largest contributions are observed for the middle monomer (monomer 3) for both variants. For exc-u-EDA, the interactions are next largest for monomers 2 and 4, and smallest for monomers 1 and 5. This consistent pattern is observed across all instances. In exc-r-EDA, monomers 1 and 5 show a notably larger increase in the orbital term compared to the electrostatic contribution, whereas for the other monomers, both contributions are similarly affected. This suggests minimal CT for monomers 1 and 5, with excitation effects more pronounced compared to monomers 2 and 4. Overall, the results confirm that the exc-EDA method exhibits the expected structural characteristics since it reflects the symmetry of the clusters. In conclusion, the EDA results suggest that the initial singlet fission event in pentacene clusters involves not only two molecules but at least four. Additionally, a CT excitation is observed at this stage, indicating that the singlet fission process in pentacene occurs *via* a CT intermediate as proposed before.[73,74]

5. Conclusion

We present a novel energy decomposition analysis method for excited states, combining the Morokuma and Ziegler-Rauk EDA approach with TDDFT. The method calculates excitation energies for intermediate EDA steps and includes two variants: exc-u-EDA, which uses fixed excitation coefficients for fragments,

and exc-r-EDA, which optimizes these coefficients with TDDFT. Tests showed that both variants provide reliable results, with exc-u-EDA being more robust but exc-r-EDA better suited for systems involving charge transfer. Hybrid functionals showed smaller values than range-separated GGA functionals and were less prone to artificial changes in excited states due to closely spaced excited states or numerous virtual orbitals. Smaller basis sets mitigate these issues by resulting in more distinct virtual orbitals. Comparing Pauli repulsion between the two variants can guide the choice of method, with lower Pauli repulsion indicating a better description of the system.

For a test set of four exciplex complexes, exc-EDA delivered quantitative bonding insights and chemically intuitive pictures. The comparison to established methods for excited state EDA shows similar trends. We further applied exc-EDA to study singlet fission in pentacene clusters, revealing charge transfer from excited to non-excited monomers, known as CT-mediated singlet fission. The interaction between fragments was slightly enhanced by excitation, driven equally by electrostatic and orbital interactions. Accurate description of excitation effects required at least a tetramer cluster model, and the method reproduced expected structural differences within excited monomers.

The exc-EDA offers a novel perspective on bonding in the excited state. This method can provide additional insights compared to more established approaches, particularly in terms of bonding analysis. As a result, it enables a more accurate and detailed understanding of the respective excited states.

The exc-EDA method is applicable to systems where the excitation is localized on one fragment and can help analyze the effect of excitation on bonding. It works across most functional classes, though care is needed to ensure the selected functional accurately describes the excitation. Double-hybrid functionals are an exception, as they are not compatible with this method.

In the future, we will use exc-EDA to analyze chemistry in the excited state.

Data availability

The data for this article and the ESI,† including all computational data as well as the scripts to create the diagrams and the diagrams, are available at Zenodo (**https://doi.org/10.5281/zenodo.14024534**). The method has been implemented in the AMS program package and should be available with the 2025 version.

Conflicts of interest

There are no conflicts to declare.

Acknowledgements

We thank SCM/Amsterdam and specifically Dr Stan Gisbergen for providing a developer's version of the AMS code. We thank Dr Eric van Lenthe for discussions. We thank the German Science Foundation (DFG) for funding *via* RTG ^{123}H (443871192).

References

1 (*a*) V. Balzani, *Photochemistry and Photophysics*, Wiley, 2014; (*b*) V. Balzani, G. Bergamini and P. Ceroni, *Angew. Chem., Int. Ed.*, 2015, **54**, 11320; (*c*) R. C. Evans, P. Douglas and H. D. Burrow, *Applied Photochemistry*, Springer, Netherlands, Dordrecht, 2013; (*d*) B. König, *Eur. J. Org. Chem.*, 2017, 1979; (*e*) S. Reischauer and B. Pieber, *iScience*, 2021, **24**, 102209.
2 A. Dreuw and M. Head-Gordon, *Chem. Rev.*, 2005, **105**, 4009.
3 (*a*) J. V. Burykina, A. D. Kobelev, N. S. Shlapakov, A. Y. Kostyukovich, A. N. Fakhrutdinov, B. König and V. P. Ananikov, *Angew. Chem., Int. Ed.*, 2022, **61**, e202116888; (*b*) A. Hölzl-Hobmeier, A. Bauer, A. V. Silva, S. M. Huber, C. Bannwarth and T. Bach, *Nature*, 2018, **564**, 240; (*c*) R. Lahmy, H. Hübner, P. Gmeiner and B. König, *ChemPhotoChem*, 2024, **8**, e202400022; (*d*) M. Leverenz, C. Merten, A. Dreuw and T. Bach, *J. Am. Chem. Soc.*, 2019, **141**, 20053; (*e*) T. E. Schirmer and B. König, *J. Am. Chem. Soc.*, 2022, **144**, 19207; (*f*) N. S. Shlapakov, A. D. Kobelev, J. V. Burykina, A. Y. Kostyukovich, B. König and V. P. Ananikov, *Angew. Chem., Int. Ed.*, 2024, **63**, e202314208; (*g*) C. Taube, J. Fidelius, K. Schwedtmann, C. Ziegler, F. Kreuter, L. Loots, L. J. Barbour, R. Tonner-Zech, R. Wolf and J. J. Weigand, *Angew. Chem., Int. Ed.*, 2023, **62**, e202306706; (*h*) A. Zech, C. Jandl and T. Bach, *Angew. Chem., Int. Ed.*, 2019, **58**, 14629.
4 S. Mai and L. González, *Angew. Chem., Int. Ed.*, 2020, **59**, 16832.
5 H. Lischka, D. Nachtigallová, A. J. A. Aquino, P. G. Szalay, F. Plasser, F. B. C. Machado and M. Barbatti, *Chem. Rev.*, 2018, **118**, 7293.
6 B. O. Roos, *Advances in Chemical Physics*, John Wiley & Sons, Ltd, 1987, pp. 399–445.
7 K. Andersson and B. O. Roos, Multiconfiguratoinal second-order perturbation theory, in *Modern Electronic Structure Theory*, 1995, pp. 55–109.
8 C. Angeli, R. Cimiraglia and J.-P. Malrieu, *J. Chem. Phys.*, 2002, **117**, 9138.
9 R. J. Buenker, S. D. Peyerimhoff and W. Butscher, *Mol. Phys.*, 1978, **35**, 771.
10 P. A. Malmqvist, A. Rendell and B. O. Roos, *J. Chem. Phys.*, 1990, **94**, 5477.
11 R. Izsák, *Wiley Interdiscip. Rev.: Comput. Mol. Sci.*, 2020, **10**, e1445.
12 J. Geertsen, M. Rittby and R. J. Bartlett, *Chem. Phys. Lett.*, 1989, **164**, 57.
13 C. Hättig and F. Weigend, *J. Chem. Phys.*, 2000, **113**, 5154.
14 A. Dreuw and M. Wormit, *Wiley Interdiscip. Rev.: Comput. Mol. Sci.*, 2015, **5**, 82.
15 M. E. Casida and M. Huix-Rotllant, *Annu. Rev. Phys. Chem.*, 2012, **63**, 287.
16 N. T. Maitra, *J. Chem. Phys.*, 2016, **144**, 220901.
17 E. Pastorczak and C. Corminboeuf, *J. Chem. Phys.*, 2017, **146**, 120901.
18 F. M. Bickelhaupt and E. J. Baerends, in *Reviews in Computational Chemistry*, ed. K. B. Lipkowitz and D. B. Boyd, Wiley-VCH, Inc., New York, 2000, vol. 15, pp. 1–86.

19 K. Kitaura and K. Morokuma, *Int. J. Quantum Chem.*, 1976, **10**, 325.
20 L. Zhao, M. von Hopffgarten, D. M. Andrada and G. Frenking, *Wiley Interdiscip. Rev.: Comput. Mol. Sci.*, 2018, **8**, e1345.
21 T. Ziegler and A. Rauk, *Theor. Chim. Acta*, 1977, **46**, 1.
22 M. Raupach and R. Tonner, *J. Chem. Phys.*, 2015, **142**, 194105.
23 A. Seidl, A. Görling, P. Vogl, J. A. Majewski and M. Levy, *Phys. Rev. B:Condens. Matter Mater. Phys.*, 1996, **53**, 3764.
24 (*a*) P. Maxwell, Á. M. Pendás and P. L. A. Popelier, *Phys. Chem. Chem. Phys.*, 2016, **18**, 20986; (*b*) M. A. Blanco, A. Martín Pendás and E. Francisco, *J. Chem. Theory Comput.*, 2005, **1**, 1096.
25 (*a*) Y. Mo, L. Song and Y. Lin, *J. Phys. Chem. A*, 2007, **111**, 8291; (*b*) Y. Mo, J. Gao and S. D. Peyerimhoff, *J. Chem. Phys.*, 2000, **112**, 5530; (*c*) Y. Mo, P. Bao and J. Gao, *Phys. Chem. Chem. Phys.*, 2011, **13**, 6760.
26 (*a*) P. R. Horn, E. J. Sundstrom, T. A. Baker and M. Head-Gordon, *J. Chem. Phys.*, 2013, **138**, 134119; (*b*) R. Z. Khaliullin, E. A. Cobar, R. C. Lochan, A. T. Bell and M. Head-Gordon, *J. Phys. Chem. A*, 2007, **111**, 8753.
27 T. M. Cardozo and M. A. C. Nascimento, *J. Chem. Phys.*, 2009, **130**, 104102.
28 (*a*) E. D. Glendening, *J. Am. Chem. Soc.*, 1996, **118**, 2473; (*b*) E. D. Glendening and A. Streitwieser, *J. Chem. Phys.*, 1994, **100**, 2900.
29 P. Su and H. Li, *J. Chem. Phys.*, 2009, **131**, 14102.
30 K. Szalewicz, *Wiley Interdiscip. Rev.: Comput. Mol. Sci.*, 2012, **2**, 254.
31 L. Pecher and R. Tonner, *Wiley Interdiscip. Rev.: Comput. Mol. Sci.*, 2019, **9**, e1401.
32 F. M. Bickelhaupt and K. N. Houk, *Angew. Chem., Int. Ed.*, 2017, **56**, 10070.
33 P. Vermeeren, T. A. Hamlin, I. Fernández and F. M. Bickelhaupt, *Chem. Sci.*, 2020, **11**, 8105.
34 (*a*) Q. Ge, Y. Mao and M. Head-Gordon, *J. Chem. Phys.*, 2018, **148**, 64105; (*b*) Q. Ge and M. Head-Gordon, *J. Chem. Theory Comput.*, 2018, **14**, 5156.
35 Z. Tang, B. Shao, W. Wu and P. Su, *Phys. Chem. Chem. Phys.*, 2023, **25**, 18139.
36 Y. Xu, R. Friedman, W. Wu and P. Su, *J. Chem. Phys.*, 2021, **154**, 194106.
37 C. P. Hettich, X. Zhang, D. Kemper, R. Zhao, S. Zhou, Y. Lu, J. Gao, J. Zhang and M. Liu, *JACS Au*, 2023, **3**, 1800.
38 Y. X. Zhang, B. L. Mali and C. D. Geddes, *Spectrochim. Acta, Part A*, 2012, **85**, 134.
39 P. Kimber and F. Plasser, *J. Chem. Theory Comput.*, 2023, **19**, 2340.
40 R. L. Martin, *J. Chem. Phys.*, 2003, **118**, 4775.
41 F. Weinhold and C. R. Landis, *Chem. Educ. Res. Pract.*, 2001, **2**, 91.
42 N. V. Tkachenko and A. I. Boldyrev, *Phys. Chem. Chem. Phys.*, 2019, **21**, 9590.
43 (*a*) S. A. Bäppler, F. Plasser, M. Wormit and A. Dreuw, *Phys. Rev. A:At., Mol., Opt. Phys.*, 2014, **90**, 52521; (*b*) C. Adamo, T. Le Bahers, M. Savarese, L. Wilbraham, G. García, R. Fukuda, M. Ehara, N. Rega and I. Ciofini, *Coord. Chem. Rev.*, 2015, **304–305**, 166.
44 (*a*) M. T. do Casal, J. M. Toldo, M. Barbatti and F. Plasser, *Chem. Sci.*, 2023, **14**, 4012; (*b*) F. Plasser, M. Wormit and A. Dreuw, *J. Chem. Phys.*, 2014, **141**, 24106.
45 G. Frenking, K. Wichmann, N. Fröhlich, C. Loschen, M. Lein, J. Frunzke and V. M. Rayón, *Coord. Chem. Rev.*, 2003, **238–239**, 55.
46 (*a*) A. Diefenbach, F. M. Bickelhaupt and G. Frenking, *J. Am. Chem. Soc.*, 2000, **122**, 6449; (*b*) M. S. Nechaev, V. M. Rayón and G. Frenking, *J. Phys. Chem. A*, 2004, **108**, 3134; (*c*) R. Tonner, G. Heydenrych and G. Frenking, *Chem. – Asian J.*, 2007, **2**, 1555.
47 (*a*) S. C. A. H. Pierrefixe and F. M. Bickelhaupt, *Chem. – Eur. J.*, 2007, **13**, 6321; (*b*) S. C. A. H. Pierrefixe and F. M. Bickelhaupt, *J. Phys. Chem. A*, 2008, **112**, 12816.
48 L. de Azevedo Santos, T. C. Ramalho, T. A. Hamlin and F. M. Bickelhaupt, *Chem. – Eur. J.*, 2023, **29**, e202203791.
49 L. P. Wolters and F. M. Bickelhaupt, *ChemistryOpen*, 2012, **1**, 96.
50 (*a*) M. Bortoli, S. M. Ahmad, T. A. Hamlin, F. M. Bickelhaupt and L. Orian, *Phys. Chem. Chem. Phys.*, 2018, **20**, 27592; (*b*) L. de Azevedo Santos, S. C. C. van der Lubbe, T. A. Hamlin, T. C. Ramalho and F. Matthias Bickelhaupt, *ChemistryOpen*, 2021, **10**, 391.
51 L. de Azevedo Santos, T. A. Hamlin, T. C. Ramalho and F. M. Bickelhaupt, *Phys. Chem. Chem. Phys.*, 2021, **23**, 13842.
52 (*a*) Z. Boughlala, C. Fonseca Guerra and F. M. Bickelhaupt, *J. Phys. Chem. A*, 2019, **123**, 9137; (*b*) Z. Boughlala, C. Fonseca Guerra and F. M. Bickelhaupt, *Chem. – Asian J.*, 2017, **12**, 2604.
53 (*a*) A. O. Ortolan, G. F. Caramori, F. Matthias Bickelhaupt, R. L. T. Parreira, A. Muñoz-Castro and T. Kar, *Phys. Chem. Chem. Phys.*, 2017, **19**, 24696; (*b*) A. O. Ortolan, I. Østrøm, G. F. Caramori, R. L. T. Parreira, E. H. Da Silva and F. M. Bickelhaupt, *J. Phys. Chem. A*, 2018, **122**, 3328.
54 S. Grimme, S. Ehrlich and L. Goerigk, *J. Comput. Chem.*, 2011, **32**, 1456.
55 S. Hirata and M. Head-Gordon, *Chem. Phys. Lett.*, 1999, **314**, 291.
56 R. B. Morgan, *J. Comput. Phys.*, 1990, **89**, 241.
57 G. te Velde, F. M. Bickelhaupt, E. J. Baerends, C. Fonseca Guerra, S. J. A. van Gisbergen, J. G. Snijders and T. Ziegler, *J. Comput. Chem.*, 2001, **22**, 931.
58 E. van Lenthe and E. J. Baerends, *J. Comput. Chem.*, 2003, **24**, 1142.
59 (*a*) A. D. Becke, *J. Chem. Phys.*, 1988, **88**, 2547; (*b*) M. Franchini, P. H. T. Philipsen and L. Visscher, *J. Comput. Chem.*, 2013, **34**, 1819.
60 (*a*) J. P. Perdew, *Phys. Rev. B:Condens. Matter Mater. Phys.*, 1986, **33**, 8822; (*b*) A. D. Becke, *Phys. Rev. A:At., Mol., Opt. Phys.*, 1988, **38**, 3098.
61 J. P. Perdew, K. Burke and M. Ernzerhof, *Phys. Rev. Lett.*, 1996, **77**, 3865.
62 T. Yanai, D. P. Tew and N. C. Handy, *Chem. Phys. Lett.*, 2004, **393**, 51.

63 Y. Tawada, T. Tsuneda, S. Yanagisawa, T. Yanai and K. Hirao, *J. Chem. Phys.*, 2004, **120**, 8425.
64 E. Epifanovsky, A. T. B. Gilbert, X. Feng, J. Lee, Y. Mao, N. Mardirossian, P. Pokhilko, A. F. White, M. P. Coons and A. L. Dempwolff, *et al.*, *J. Chem. Phys.*, 2021, **155**, 84801.
65 F. Weigend and R. Ahlrichs, *Phys. Chem. Chem. Phys.*, 2005, **7**, 3297.
66 P. M. Zimmerman, Z. Zhang and C. B. Musgrave, *Nat. Chem.*, 2010, **2**, 648.
67 A. Neef, S. Beaulieu, S. Hammer, S. Dong, J. Maklar, T. Pincelli, R. P. Xian, M. Wolf, L. Rettig and J. Pflaum, *et al.*, *Nature*, 2023, **616**, 275.
68 L. Craciunescu, S. Wirsing, S. Hammer, K. Broch, A. Dreuw, F. Fantuzzi, V. Sivanesan, P. Tegeder and B. Engels, *J. Phys. Chem. Lett.*, 2022, **13**, 3726.
69 Y.-S. Lin, G.-D. Li, S.-P. Mao and J.-D. Chai, *J. Chem. Theory Comput.*, 2013, **9**, 263.
70 T. Oestereich, R. Tonner-Zech and J. Westermayr, *J. Comput. Chem.*, 2024, **45**, 368.
71 G.-J. Zhao and K.-L. Han, *J. Phys. Chem. A*, 2007, **111**, 9218.
72 (*a*) Y. Mei and W. Yang, *J. Chem. Phys.*, 2019, **150**, 144109; (*b*) J. M. Masnovi, E. A. Seddon and J. K. Kochi, *Can. J. Chem.*, 1984, **62**, 2552.
73 B. S. Basel, J. Zirzlmeier, C. Hetzer, S. R. Reddy, B. T. Phelan, M. D. Krzyaniak, M. K. Volland, P. B. Coto, R. M. Young and T. Clark, *et al.*, *Chem*, 2018, **4**, 1092.
74 R. Casillas, I. Papadopoulos, T. Ullrich, D. Thiel, A. Kunzmann and D. M. Guldi, *Energy Environ. Sci.*, 2020, **13**, 2741.